Published in final edited form as:
Adv Genet. 2010 ; 69: 31–64. doi:10.1016/S0065-2660(10)69009-8.

An Integrated Approach for the Rational Design of NanoVectors for Biomedical Imaging and Therapy

Biana Godin[1], **Wouter H. Driessen**[2], **Bettina Proneth**[2], **Sei-Young Lee**[1], **Srimeenakshi Srinivasan**[1], **Rolando Rumbaut**[3], **Wadih Arap**[2], **Renata Pasqualini**[2], **Mauro Ferrari**[1,4], and **Paolo Decuzzi**[1,5]

[1]Department of Nanomedicine and Biomedical Engineering, The University of Texas Health Science Center at Houston; Houston TX-USA

[2]Department of Genitourinary Medical Oncology and Department of Cancer Biology; The University of Texas M. D. Anderson Cancer Center; Houston, TX – USA

[3]Children's Nutrition Research Center; Baylor College of Medicine Houston, TX - USA

[4]Department of Experimental Therapeutic; The University of Texas M. D. Anderson Cancer Center; and Department of Biomedical Engineering; Rice University; Houston, TX - USA

[5]Center of Bio-/Nanotechnology and -/Engineering for Medicine; University of Magna Graecia; Catanzaro - ITALY

Abstract

The use of nanoparticles for the early detection, cure and imaging of diseases has been proved already to have enormous potentials in different biomedical fields, as oncology and cardiology. A broad spectrum of nanoparticles are currently under development exhibiting differences in (i) size, ranging from few tens of nanometers to few microns; (ii) shape, from the classical spherical beads to discoidal, hemispherical, cylindrical and conical; (iii) surface functionalization, with a wide range of electrostatic charges and bio-molecule conjugations. Clearly, the library of nanoparticles generated by combining all possible sizes, shapes and surface physico-chemical properties is enormous. With such a complex scenario, an integrated approach is here proposed and described for the rational design of nanoparticle systems (nanovectors) for the intravascular delivery of therapeutic and imaging contrast agents. The proposed integrated approach combines multi-scale/multi-physics mathematical models with in-vitro assays and in-vivo intravital microscopy experiments and aims at identifying the optimal combination of size, shape and surface properties that maximize the nanovectors localization within the diseased microvasculature.

I. Introduction

The use of nanoparticles as carriers for therapeutic and imaging contrast agents is based on the concurrent, expected advantages of homing at the diseased site (as cancer lesions), and the ability to bypass the biological barriers encountered between the point of administration and the target tissue. Oncology is the field of medicine where the contribution of nanotechnology has been well established for the last decade (Heath and Davis, 2008; Nie et al., 2007; Riehemann et al., 2008) Liposomes are the most investigated drug-delivery nanoparticle and commercially available since 1996, when liposomal doxorubicin had been

granted FDA approval for use against Kaposi's sarcoma. Currently it is also approved for treatment of metastatic breast cancer and recurrent ovarian cancer.

Since then a plethora of nanoparticle-based drug delivery systems have been presented and are being developed with different features and multiple-functionalities (Wang et al, 2008; Ferrari, 2005). These exhibit differences in (i) sizes, ranging from few tens of nanometers (as for dendrimers, gold and iron-oxide nanoparticles) to few hundreds of nanometers (as for polymeric and lipid-based particles) to micron-sized particles; (ii) shapes, from the classical spherical beads to discoidal, hemispherical, cylindrical and conical; (iii) surface functionalizations, with a broad range of electrostatic charges and bio-molecule conjugations. Clearly, the library generated by combining all possible sizes, shapes and surface physico-chemical properties of the nanoparticles currently under development is enormous and this leads naturally to posing the following question: is there any optimal combination that could maximize the accumulation of intravascularly injected nanoparticles at the biological target site (as the cancer lesion) whilst minimizing their sequestration by the reticulo-endothelial system (RES)?

In this chapter, an integrated approach is proposed to tackle such a problem which is based on combining together mathematical models, in-vitro characterization assays and in-vivo experiments. The chapter is organized as follows: after the introduction, in the second paragraph, the different types of nanoparticle-based delivery systems so far developed are reviewed chronologically and three different generations are presented as a possible classification method; in the third paragraph, the mathematical models used to predict the behavior of intravascularly injected nanoparticles are presented focusing the attention on their transport within an authentically complex vascular system and specific/non-specific interaction with cells of the immune systems (RES cells) as well as cells lining the blood vessel walls (endothelial cells); in the following paragraph, the assays used for characterizing the geometrical and surface physico-chemical properties of the nanoparticles are reviewed with an emphasis on those properties that mostly affect the behavior of the nanoparticles in-vivo as from the mathematical predictions; in the fifth paragraph, different strategies for targeting the injected nanoparticles to the diseased vasculature are presented including the use of phage-display peptides and other conventional ligands; in the sixth part, an in-vitro assays for characterizing the dynamics, adhesive and internalization performances of nanoparticles underflow are described based on the use of parallel plate flow chamber systems; and finally in the seventh paragraph, the powerful technique of intravital video microscopy for monitoring the in-vivo behavior of the nanoparticles within the diseased vasculature is presented. The cross-interaction within the different components of the proposed integrated approach for the rational design of nanoparticle-based delivery systems is discussed in the closing paragraph.

II. Three generations of nanovectors

Nanovectors can be generally organized into three main sub-classes or 'generations' as schematically shown in Fig. 1 (Sanhai et al., 2008; Ferrari, 2005; Harris and Chess, 2003). In the sequel, the term nanovector will be used to identify systems having nanoscale components for the delivery of therapeutic or contrast agent; and the term targeting will be

used only when mentioning the specific binding of particles to the site (e.g., due to the presence of mAb on the particle's surface). When describing passive concentration governed by physical laws the terms "homing", "localization" or "direction" will be used.

II.A The first generation of nanovectors

The first generation of nanovectors (Fig. 1a) encompasses a delivery system that localizes into the lesion through passive mechanisms. Liposomes, as the liposomal doxorubicin, home within the tumor tissue mainly through the Enhanced Permeation and Retention (EPR) mechanism. The highly permeable neovasculature of the tumor, characterized by intra- and inter-endothelium openings large as several hundreds of nanometers, favor the extravasation of nanovectors which simply cross the large vascular fenestrations. These carriers can also be modified with a polyethylene glycol (PEG) or "stealth" which prevents their uptake by the reticulo endothelial system (RES), thus substantially prolonging the particles' circulation time (Harris and Chess, 2003) and increasing the likelihood of tumor homing (Maeda et al., 2000; Duncan, 2006; Torchilin, 2005). The localization in this case is driven only by the particles' nanodimensions, and is not related to any specific recognition of the tumor or neovascular targets. Nonetheless, localization through EPR has been quite successful in particular in changing the pharmacokinetic behavior, bioavailability and toxicity of the delivered drug. Myocet (non-PEGylated liposomes) and Doxil (PEGylated liposomes) were among the first liposomal systems in clinical use (Torchilin, 2005; Drummond et al., 1999). For the liposomal encapsulated doxorubicin, the elimination half-life for the free drug is only 0.2 h, but this increases to 2.5 and 55 h, respectively, when non-PEGylated and PEGylated liposomal formulations. Moreover, the area under the time–plasma concentration profile (the AUC), which indicates the bioavailability of an agent following its administration, is increased 11- and 200-fold for Myocet and Doxil, respectively, compared to the free drug (Hofheinz et al., 2005). Encapsulation into the liposomal carrier also causes a significant reduction in the most significant adverse side effect of doxorubicin, namely cardiotoxicity, as demonstrated in clinical trials (Torchilin, 2005; Drummond et al., 1999; Hofheinz et al., 2005; Parveen and Sahoo, 2006). Other liposomal drugs which are either currently in use or are being evaluated in clinical trials include non-PEGylated liposomal daunorubicin (DaunoXome) and vincristine (Onco-TCS), PEGylated liposomal cisplatin (SPI-77) and lurtotecan (OSI-211) (Zhang et al., 2007; Peer et al., 2007).

Within the first generation of nanovectors, metal nanoparticles for use in diagnostics, albumin paclitaxel nanoparticles approved for use in metastatic breast cancer, and drug–polymer constructs are also included (Zhang et al., 2007; Peer et al., 2007; Gradishar et al., 2005; Ringsdorf, 1975; Vasey et al., 1999; Allen, 2002).

II.B The second generation of nanovectors

The second generation of nanovectors encompasses delivery systems with additional functionality including surface moieties on the nanovector, providing specific molecular recognition of receptors expressed over the tumor cells or within the tumor vasculature (Fig. 1b), and active/triggered release of the payload at the diseased location. The most investigated example of the second generation nanovectors are antibody-targeted nanoparticles, such as mAb-conjugated liposomes (Brannon-Peppas and Blanchette, 2004;

Torchilin, 2007; Saul et al., 2006; Yang et al., 2006; Souza et al., 2006; Maeda et al., 2000; Allen, 2002; Juweid et al., 1992; Banerjee et al., 2001; Adams et al., 2001; Goren et al., 1996; Langer, 1998). A variety of targeting moieties besides antibodies are under extensive investigation worldwide, including ligands, aptamers, small peptides and phage-display peptide binding to specific target cell-surface markers or surface markers expressed in the disease microenvironment and these will be further discussed in our Chapter (Kang et al., 2008; Hajitou et al., 2006).

The choice between high or low binding affinity of the ligand for its antigen or receptor remains an issue still to be resolved. Within the tumor, when the binding affinity is high, there is some evidence that the penetration of targeted therapeutics into a cancerous mass is drastically reduced due to the 'binding-site barrier'. In this case the targeted therapeutics binds strongly to the first targets encountered, but fails to diffuse further into the tumor. On the other hand, for targets in which most of the cells are readily accessible to the delivery system – for example, tumor vasculature and certain hematological malignancies – a high binding affinity is desirable.

As regarding responsive drug delivery systems, pH- or enzyme-sensitive polymers as well as a diverse group of remotely activated nanovectors have been demonstrated. Among the most interesting examples here are gold nanoshells that are activated by near-infrared light, or iron oxide nanoparticles triggered by oscillating magnetic fields (Duncan, 2003; Hirsch et al., 2003). Linking nanoshells to antibodies that recognize cancer cells enables these novel systems to seek out their cancerous targets prior to applying near-infrared light to heat them up. For example, in a mouse model of prostate cancer, nanoparticles activated with fluoropyrimidine RNA aptamers that recognized the extracellular domain of the PSMA, and loaded with docetaxel as a cytostatic drug, were used for targeting and destroying cancer cells (Farokhzad et al., 2006a; Farokhzad 2006b). Other techniques used to remotely activate the second-generation particulates include ultrasound and radiofrequency (Douziech-Eyrolles et al., 2007; Schroeder et al., 2007; Monsky et al., 2002). Although the representatives of the second generation have not yet been approved by FDA, there are numerous ongoing clinical trials involving targeted nanovectors, especially in cancer applications.

Compared to their predecessors, the second-generation nanoparticles offered new degrees of sophistication by employing additional complexities such as targeting moieties, remote activation, and environmentally sensitive components. Predominantly, the second generation represents simply a progressive evolution of the first-generation nanovectors. The subtle, yet augmenting, improvements described above do not fully address the primary challenge – or set of challenges – presented in the form of sequential biological barriers that continue to impair the efficacy of delivery systems. This fundamental problem has given rise to a paradigm shift in the design of nanoparticles with the emergence of a third generation of particle that is specifically engineered to avoid biological barriers and to co-deliver multiple nanovector payloads with tumor specificity. The ideal injected chemotherapeutic strategy is envisioned to be capable of navigating through the vasculature after intravenous administration, to reach the desired tumor site at full concentration, and to selectively kill cancer cells with a cocktail of agents with minimal harmful side effects.

II.C The third generation of nanovectors

Third generation nanovectors (Fig. 1c), such as multistage agents, are capable of more complex functions which enable sequential overcoming of multiple biobarriers. An example is the time-controlled release of multiple payloads of active nanoparticles, negotiating different biological barriers and with different subcellular targets (Sakamoto et al., 2007). This generation of nanovectors represent the first wave of next-generation nanotherapeutics that are specifically equipped to address biological barriers to improve payload delivery at the tumor site. Some of the above-mentioned and most notable challenges include physiological barriers (i.e. the RES, epithelial/endothelial membranes, cellular drug extrusion mechanisms) and biophysical barriers (i.e. interstitial pressure gradients, expression and density of specific tumor receptors, and ionic molecular pumps). Biobarriers are sequential in nature, and therefore the probability of reaching the therapeutic objective is the product of individual probabilities of overcoming each and every one of them (Ferrari, 2005). By definition, third-generation nanoparticles have the ability to perform a time sequence of functions which involve the cooperative coordination of multiple nanoparticles and/or nanocomponents. This novel generation of nanotherapeutics is exemplified through the employment of multiple nanobased products that synergistically provide distinct functionalities. Here, the nanocomponents will include any engineered or artificially synthesized nanoproducts, such as peptides, oligonucleotides (e.g. thioaptamers, siRNA) and phage with targeting peptides. Naturally existing biological molecules, e.g. antibodies, will be excluded from this designation, despite their ability to be synthesized.

Third-generation nanovectos have been developed to address the numerous challenges responsible for reducing the chemotherapeutic efficacy of earlier strategies. For example, surface modification of the exterior of nanoparticles with PEG has proven to be effective in increasing the circulation time within the bloodstream; however, this preservation tactic proves detrimental to the biological recognition and targeting ability of the nanovector (Klibanov et al., 1991). In order to avoid such contradictory approaches of employing incapacitating improvements to therapeutic delivery systems, many research groups are combining multiple nanotechnologies to exploit the additive contributions of the constituent components. One example of third-generation nanoparticles is the biologically active molecular networks known as ‘nanoshuttles’ (Souza et al., 2008). These self-assemblies of gold nanoparticles within a bacteriophage matrix combine the biological targeting capabilities phage-display peptides with hyperthermic response to near-infrared radiation, CT imaging contrast and surface-enhanced Raman scattering detection of the gold nanoparticles.

The next example of third-generation nanoparticles is the disease-inspired approach of the ‘nanocell’, which are nested nanoparticle constructs that comprise a lipid-based nanoparticle enveloping a polymeric nanoparticle core. In this case, a conventional chemotherapeutic drug (e.g. doxorubicin) is conjugated to a polymer core and an anti-angiogenic agent (combretastatin) is then trapped within the lipid envelope. When the nanocells are accumulated within the tumor through the EPR effect, the sequential time release of the anti-angiogenic agent, followed by the cytotoxic drug, causes an initial disruption of tumor

vascular growth and effectively traps the drug-conjugated nanoparticle core within the tumor to allow an eventual delivery of the cancer cell-killing agent (Sengupta et al., 2005).

The final example of third-generation nanoparticle technology utilizes a multistage approach that addresses many biological barriers experienced by an injectable therapy. Currently, research groups are developing nanoporous silicon microparticles that utilize their unique particle size, shape and other physical characteristics in concert with active tumor biological targeting moieties to efficiently deliver payloads of nanoparticles to the tumor site, resolving mission-critical issues that must be addressed in a sequential manner when developing drug delivery systems to fight cancer. The multistage drug delivery system is predicated upon a Stage 1 nanoporous silicon microparticle that is specifically designed (through mathematical modeling) to exhibit superior margination and adhesion properties during its negotiation through the systemic blood flow en route to the tumor site. Particle characteristics such as size, shape, porosity and charge can be exquisitely controlled with precise reproducibility through microfabrication techniques. In addition to its favorable physical characteristics, the Stage 1 particle can be surface-treated with such modifications as PEG for RES avoidance and also equipped with biologically active targeting moieties (e.g. aptamers, peptides, phage, antibodies) to enhance the tumor vasculature targeting specificity. This approach decouples the challenges of: (i) transporting therapeutic agents to the tumor-associated vasculature; and (ii) delivering therapeutic agents to cancer cells. The Stage 1 particles shoulder the burden of efficiently transporting a nanoparticle payload to the adjacent tumor vasculature within the nanoporous structures of its interior, serving as a cargo for the Stage 2 nanoparticles. Stage 2 particles, generically represent any nanodimention construct within the approximate diameter range of 5 to 100 nm and can be efficiently loaded into the Stage 1 particles with gradual release profile (Tasciotti et al., 2008). The multistage drug delivery system is emblematic of third-generation nanoparticle technology, since the strategy combines numerous nanocomponents to deliver multiple nanovectors to a tumor lesion. The Stage 1 particle is rationally designed to enhance particle margination within blood vessels, and to increase particle/endothelium interaction for enhancing the probability of active tumor targeting and adhesion (Ferrari 2008). In addition to improved hemodynamic physical properties and active biological targeting by utilizing nanocomponents such as aptamers and phage, the Stage 1 particle can also present with specific surface modifications in order to avoid RES uptake and exhibit degradation rates predetermined by nanopore density. Upon tumor recognition and vascular adhesion, a series of nanoparticle payloads may be released in a sequential order predicated upon Stage 1 particle degradation rates and payload conjugation strategies (e.g. environmentally sensitive crosslinking techniques, pH, temperature, enzymatic triggers). The versatility of this platform nanovector multistage delivery particle allows for a multiplicity of applications. Depending upon the nanoparticle ‘cocktail’ loaded within the Stage 1 particle, this third-generation nanoparticle system can provide for the delivery not only of cytotoxic drugs but also of remotely activated hyperthermic nanoparticles, contrast agents and future nanoparticle technologies.

III. Mathematical Models for predicting the Nanovectors’ behavior

Inspired by the behavior of circulating blood cells, as leukocytes and platelets, the dynamics of an intravascularly injected nanovector can be broken down into three main events,

extensively described by Decuzzi and collaborators (Decuzzi et al., 2009): (i) transport and margination dynamics along the vascular network, (ii) firm adhesion to the vascular endothelium and (iii) control of internalization/translocation across the vascular endothelium. The size, shape and surface physico-chemical properties of nanovectors have been shown to affect, at different extent, each of these three basic events, as described in the sequel. A multi-scale multi-physics mathematical model is required to predict the behavior of intravasculalry injected nanovectors combining *three modules*: (i) a *transport module* for the analysis of nanovector transport within an authentically complex vascular network; (ii) a *margination and adhesion module* for analyzing the near-wall dynamics of a single nanovector including the margination dynamics and firm adhesion to the vessel walls; and (iii) an *uptake module* for analyzing the possible internalization of nanovectors by RES and endothelial cells.

III.A Modeling the transport within the authentic vasculature

The *Transport Module* analyzes the convective and diffusive transport of nanovectors within an authentically complex vascular network in the presence of blood flow. In the absence of external forces other than the hydrodynamic forces associated with blood flow, the 3D advective-diffusive equation can be employed

$$\frac{\partial C}{\partial t}+\nabla\cdot(\boldsymbol{V}C)=\nabla\cdot(\nabla DC) \quad (1)$$

where C is the volume concentration of nanovectors; t is the time; V is the local fluid velocity; D is the molecular diffusion coefficient of nanovectors in a quiescent fluid, and ∇ and $\nabla\cdot$ are respectively the gradient and divergence operators. The flow field is derived by solving the momentum and mass conservation equations for a non-Newtonian fluid

$$\rho\frac{D\boldsymbol{V}}{Dt}=\nabla\cdot(\mu\nabla\boldsymbol{V})-\nabla p \quad \nabla\cdot\boldsymbol{V}=0 \quad (2)$$

where ρ is the density of the fluid, p is the hydrodynamic pressure within the vascular network and μ is the apparent viscosity for a Casson fluid, given by

$$\mu=\left[K_c+\left(\tau_o/\sqrt{(\nabla\cdot\boldsymbol{V})^2}\right)^{1/2}\right]^2 \quad (3)$$

with K_c the Casson's coefficient of viscosity and τ_0 the yield stress of the fluid (Fung, 1993). The Casson model has been widely used for reproducing the rheological properties of blood. Although more complex approaches and rheological laws could be used, the Casson model represents a good compromise between computational efficiency and accuracy of the results (Neofytou, 2004).

The system of equations (1) to (3) is closed by imposing the proper initial and boundary conditions. For the flow field, a characteristic velocity profile, varying with time, is imposed

at the inlet of the vascular network and a reference zero pressure is imposed at the outlet of the vascular network, whereas on the vessel surfaces the classical Starling's law (Jain, 1987) can be imposed

$$v_n = L_p \left[(p_c - p_i) - \sigma \Delta \pi \right] \quad (4)$$

introducing the wall hydraulic conductivity L_p, the hydrostatic capillary pressure p_c and interstitial fluid pressure p_i; the osmotic reflection coefficient σ; and the oncotic pressure difference between the vessel and the interstitial compartment $\Delta\pi$; and the fluid velocity normal to the vessel wall v_n. The case of an impermeable wall can be readily obtained by imposing L_p=0. The model allows to account for the permeability of the vessel walls which varies from organ to organ being very small in the brain vasculature and extraordinary large within the RES organs, as the spleen and the liver, and within the tumor vasculature. Physiologically relevant data for L_p are summarized in Tab. 1.

For the transport equation, the auxiliary conditions are a characteristic concentration profile, varying with time, at the inlet and a reference zero concentration at the outlet of the vascular network. On the permeable vessel surface, a Starling-like boundary condition is imposed, whereas on the remaining portion impermeable boundary conditions including the adhesion K_a and decohesion K_d rates can be introduced to account for the nanovector adhesion and detachment under flow.

The boundary value problem described above allows for the analysis of the transport, adhesion and extravasation of nanovectors within an authentic complex vascular network. The independent parameters that can be changed and that affect the performance of the nanovector in vivo are: i) the geometry of the network, as the vessel diameter, length, tortuosity and branching type and level; ii) the hydrodynamic conditions as the mean blood velocity; iii) the permeability of the vessel walls to fluid and nanovectors, which could vary within the network; iv) the adhesiveness of the vessel walls to nanovectors. As an example, Fig. 2 shows the transport and adhesion of nanovectors within a tortuous vessel with a branch. For oncological applications, a list of physiologically relevant values of the biophysical parameters needed for running the simulations of Fig. 2 are listed in Tab. 2.

III.B Modeling the margination and adhesion dynamics of nanovectors

Red blood cells (RBCs) tend to preferentially accumulate within the core of the vessels, because of their shape and more importantly deformability under flow, leaving a 'cell free layer' in proximity of the wall (Sharan and Popel, 2001; Kim et al., 2007). The endothelial cell glycocalyx, a network containing glycoproteins and proteoglycans bound to the luminal cell membrane, contributes to the RBC-free layer and is increasingly recognized as a physiologically relevant structure. The cell free layer has a thickness varying with the vessel lumen and mean blood velocity and ranging from ~0.5 μm in small capillaries (5 μm and more in diameter) to several microns in arterioles (100 μm and more in diameter) (Sharan and Popel, 2001; Kim et al., 2007). Since nanovectors are supposed to inspect the vessel walls seeking for biophysical and biological diversities, as for instance the presence of endothelial fenestrations or an over-expression of specific receptor molecules, they should

be rationally designed to accumulate in the cell free layer. In other words, nanovectors should be rationally designed to marginate under the action of the hydrodynamic forces. Margination is a well-known term in physiology used to describe the lateral drift of leukocytes and platelets towards the endothelial walls, a process that enhances the likelihood of interaction of these circulating cells with the vascular walls. However, whilst leukocyte and platelets margination is an active process requiring an interaction with red blood cells and the dilatation of the inflamed vessels and consequent blood flow reduction (Goldsmith and Spain, 1984); particle margination can only be achieved by proper rational design. Within the cell free layer a linear laminar flow exists with a shear rate S, and under such hydrodynamic conditions it has been shown that spherical nanovectors tend to follow the streamlines without drifting towards the vessel walls (Goldman et al., 1967). Only external gravitational and magnetic forces can deviate the spherical beads from following the streamlines (Decuzzi et al., 2005). Differently, non-spherical particles with sufficient inertia have been shown to drift laterally towards the vessel wall within a linear laminar flow (Fig. 3). Clearly, a marginating particle has a larger probability of interacting with the vessel walls, but not necessarily this implies firm adhesion. The propensity for firm adhesion to the vessel walls under flow is related to the probability of adhesion P_a, which is affected by the local hydrodynamic conditions (wall shear rate S); density of the ligand molecules (m_l) distributed over the particle; density of receptor molecules (m_r) expressed on the cell membrane; non-specific interactions at the cell/particle interface (van der Waals, steric, double layer electrostatic); and particle size and shape (Decuzzi et al., 2004, Decuzzi and Ferrari 2006). Decuzzi and colleagues have demonstrated that oblate spheroidal particles (Decuzzi and Ferrari 2006) exhibit a much higher strength of adhesion (P_a) compared to spherical particles under the same hydrodynamic and biophysical conditions. In Fig. 4, the probability of adhesion is plotted versus the volume of the particle for an oblate spheroid with different aspect ratios γ ranging from unity (spherical particle) to $\gamma = 9$ for which the spheroid degenerates into an almost flat discoidal particle (see bottom of Fig. 4). The higher propensity of non-spherical particles to marginate and adhere more strongly to a substrate under flow has been also verified experimentally in-vitro, as in Fig. 5, where the number of particles depositing over a layer of fibronectin under a laminar flow in a parallel plate flow chamber has been measured for three different particle geometries (sphere, quasi-hemisphere and discoidal particles) and different shear rates S.

The Margination and Adhesion Module studies the dynamics of a single nanovector in a linear laminar flow in close proximity of the vessel walls, as within the cell free layer, accounting for the effect of nanovector size, shape and specific/non-specific interactions as well as the contribution of external forces, as gravitational and magnetic. A Lagrangian approach will be used to track particle motion whit the Newtonian governing equations

$$m\frac{d\boldsymbol{u}}{dt}=\boldsymbol{F} \quad ; \quad I\frac{d\boldsymbol{\omega}}{dt}-I\boldsymbol{\omega}\times\boldsymbol{\omega}=\boldsymbol{T} \quad (7)$$

where m and I are the mass and rotational inertia of the particle, respectively; u is the particle velocity vector and ω is the particle rotational velocity vector; F and T are the force vector and torque exerted over the particle including both surface forces, as the

hydrodynamic forces, and external mass forces, as gravitation and magnetic forces. Once the nanovector is in close proximity to the vessel wall (few tens of nanometers), the generalized forces *F* and *T* also include the contribution of non-specific interactions, as van der Waals, double layer electrostatic and steric interactions (as for the case of spherical particles in (Decuzzi et al., 2005)); and of specific interactions, based on the formation/breakage of ligand-receptor bonds as described below.

III.C Modeling the cellular internalization of nanovectors

The rate of uptake is affected by the geometry and surface physico-chemical properties of the nanovector. This has been clearly shown for spherical particles, where the size (radius) not only affects the uptake rate, but it also affects the uptake mechanisms (Rejman et al., 2004; Koval et al., 1998; Herant et al., 2006). Based on these experimental results, the rate of uptake can be described through a first order kinetic law where the intracellular concentration $C_i(t)$ grows in time following the relationship

$$\frac{d\tilde{C}_i(t)}{dt}=k_{\text{int}}\left[\chi-\tilde{C}_i(t)\right] \qquad k_{\text{int}}=\tau_w{}^{-1} \quad (9)$$

where τ_w is the characteristic time for the nanovector to be wrapped by the cell membrane, which can be related to the size, shape and surface physico-chemical properties of the nanovector as explained in the sequel. A mathematical model for receptor-mediated internalization based on an energetic analysis shows that a threshold particle radius exists below which uptake does not occur because it's energetically unfavorable. The same analysis shows that the surface physico-chemical properties of the nanovector related to that of the cell membrane can dramatically increase or decrease the uptake rate (Decuzzi and Ferrari, 2009). More recently the effect of particle shape has been also considered by several researchers (Champion and Mitragotri, 2006; Jiang et al., 2008). A mathematical model has been developed to predict the rate of uptake for ellipsoidal particles as a function of their aspect ratio Γ, as shown in Fig. 6. Spherical or ovoidal particles can be more rapidly internalized by cells compared to elongated particles. These results clearly emphasize the importance of size, shape and surface physico-chemical properties in controlling the rate of uptake of nanovectors.

III.D The adhesion maps for selecting the optimal nanovector

The Transport, Margination, Adhesion and Uptake analysis are then integrated together to generate Design Maps which recapitulate the performances of nanovectors in terms of transport, specific recognition and adhesion, and uptake as a function of the design parameters and physiological/biophysical conditions. Design Maps have been generated in the simpler case of spherical particles as a function of the non-specific interaction factor F, which accounts for the steric and electrostatic surface interactions between the particle and a cell; and of the ratio β between the number of ligand molecules distributed over the particle surface and the number of receptor molecules expressed over the cell membrane. A representative diagram is shown in Fig. 7 for fixed hydrodynamic conditions and ligand-receptor interactions. As a function of *F* and *β*, the Design Maps allow for estimating the

propensity of a circulating nanovector to adhere to a specific vascular target without being internalized by the endothelial cells, or being internalized or even avoiding any adhesion to the endothelial cells (Decuzzi and Ferrari, 2008).

IV. Biophysical characterization of nanovectors

The geometrical and physico-chemical properties of nanovectors are of prime importance for their performance, thus it is vital to characterize drug delivery particles for parameters such as particle size, size distribution, density, surface area, porosity, solubility, surface charge density, purity, surface chemistry, and stability (Donaldson and Borm, 2007). A number of techniques are intrinsically well-suited for the characterization of nanoparticles. Methods that are being employed today include among others electron microscopy (transmission and scanning), atomic force microscopy, X-ray diffraction, dynamic light scattering and laser light diffraction, BET, gas pycnometry and particle sedimentation by gravitation (Donaldson and Borm, 2007). In particular, particle size distribution may be determined by gravitational and centrifugal methods, photon correlation spectroscopy, hydrodynamic chromatography, light scattering methods, electron microscopy methods. (Donaldson and Borm, 2007; Amiji, 2005) Shape determination has been possible due to advances in image processing techniques that use shape descriptors, geometric and dynamic that carry important information to compare shapes of known and unknown particles obtained utilizing high resolution microscopy. (Donaldson and Borm, 2007)

There are advantages and limitations for any of the used techniques and these should be carefully considered. As an example, detailed information of particle sizes, shapes and agglomeration can be obtained by high resolution microscopy methods, but these are not robust techniques which are problematic for statistically reliable sampling. In fact, to enable analysis of average diameter and size distribution of the particles, the large number of micrograph sample should be processed by an image analyzing software. Most commonly used high resolution microscopy techniques are scanning and transmission electron microscopy (SEM and TEM), cryofracture, atomic force microscopy (AFM) and environmental scanning electron microscopy, which also provides information on the elemental analysis of the particle surface (Ruozi et al., 2005; Mohammed et al., 2004). In some cases various techniques are used to aid in obtaining better resolution images. For example, in SEM analysis, gold sputtering of the sample is frequently utilized to minimize fluctuations of the image thus increasing resolution. In TEM, negative staining is often employed for lipid particles, and involves a deposition of an electron opaque metal film (e.g. molybdate) on the sample. The images than appear as bright structures on dark background (a colloidal carbon coated grid) (Philippot and Schuber, 1995).

On the other hand, techniques such as dynamic light scattering (DLS), which is based on photon correlation spectroscopy, for analysis of particles size distribution provide us with statistically relevant data. However, in this case, measuring mean particle size, that is, hydrodynamic diameter determined by batch-mode dynamic light scattering in aqueous suspensions, doesn't give us any information on particles shape and morphology. The DLS method is based on analysis of the time dependence of fluctuations in the intensity of scattered light that results from the Brownian motion of the particulate object in liquid

media (Zuidam et al., 2003). The hydrodynamic radius of the object is calculated from the Stocks-Einstein equation, where particle diffusion constant (D) depends on the fluctuations of the diffused light detected by photomultiplier and is in direct relationship with particle dimensions. Particle size distribution can also be determined by gravitational and centrifugal methods, photon correlation spectroscopy and hydrodynamic chromatography (Barth, 1984; Gotoh et al., 1997; Korgel et al., 1998; Peltonen and Hirvonen, 2008). Particle size is an important physicochemical parameters that affects particles distribution as well as drug loading and release; small particles have a larger surface area, where drugs are usually found and hence lead to fast drug release, while large particles can encapsulate the drug in a core and release it in a slow time dependent manner. Particles dimensions also have an impact on the ability to cross the endothelial barrier and accumulate in various tissues and organs as will be further discussed in this chapter.

Using the DLS technique, we are able to measure another parameter that plays a pivotal role in biological interactions of the nano and micro-particles, their ζ-potential, which is the potential difference between the dispersion medium and the stationary layer of fluid attached to the dispersed particle. Zeta potential is not measurable directly but it can be calculated using theoretical models and an experimentally-determined electrophoretic mobility or dynamic electrophoretic mobility. The electrophoretic mobility and, thus the ζ-potential can be derived from the Doppler shift in frequency of light that is scattered from the particles moving in electric field (Zuidam et al., 2003). The electrostatic properties of the particles depend on the concentration of ions in the solution, the pH of the solution and the presence of multivalent ions. Other techniques that can be used for electrophoretic mobility measurements are microelectrophoresis and the electroacoustic effects such as colloid vibration current and electric sonic amplitude (Zuidam et al., 2003). ζ-potential measurement brings detailed insight and understanding of the electrokinetic magnitude of the repulsion or attraction between particles in suspension, a degree of agglomeration, particles opsonization, attachment to biological membranes, engulfment by various cells and finally particles biodistribution, toxicity and targeting ability.

Particles surface can be modified on their surface with different chemically and biologically active molecules and structures. As an example, hydrophobic particles are quickly opsonized and phagocytosed by the mononuclear phagocyte system, such as the liver, spleen, lungs and bone marrow, thus, to increase the blood circulation time, particles can be coated with flexible hydrophilic polymers (like polyethylene glycol), which shield the particles from the RES system (Stolnik et al., 1995). Active targeting to the diseased site with ligands that recognize specific molecular signatures is currently under extensive research. It can be done through attachment of antibodies, ligands, small peptides or phage-display peptide binding to specific target cell-surface markers or surface markers expressed in the disease microenvironment. There are different techniques available for characterizing the surface conjugated particles and the number of binding sites on the surface of a particle. Among these are fluorimetry, fluorescent and confocal microscopy, scintillation counting, FACS, colorimetry, XPS, AFM and PCR.

V. Vascular targeting moieties

Tumor-selective delivery is a much sought-after capability of nanovectors. Target homing strategies can be broadly divided into two categories: passive accumulation and active targeting (Seymour, 1992; Allen et al., 1995; Tyle and Ram, 1990). Passive accumulation strategies take advantage of certain unique characteristics of blood vessels in solid tumors; including factors that increase the permeability of vessels (e.g. production of factors mediating vascular permeability such as VEGF (Senger et al., 1983; Leung et al., 1989), nitric oxide (Maeda et al., 1994) and matrix metalloproteases) and the impaired lymphatic clearance of macromolecules and lipids from interstitial tumor tissue leading to enhanced retention. These effects have been well characterized and described over the past years and have been termed the enhanced permeability and retention (EPR) effect. (Maeda et al., 2003) Although it is possible to design nanovectors in a way that enhanced tumor-uptake due to the EPR-effect is achieved by decorating the particle with polymers such as PEG and HPMA (Andersson et al., 2005), a more rational approach to achieve tumor-selective delivery of nanovectors is active targeting to the vasculature. In this strategy, particles are directed to receptors over-expressed in the tumor microenvironment. As opposed to passive accumulation, this strategy strives to specifically deliver payloads by tumor endothelial cell-surface recognition. Because of the active angiogenesis process and the high vascular density in tumor-tissue, tumor endothelial cells provide a large target-area, which is readily accessible after systemic administration. Moreover, endothelial cells are genetically stable compared to tumor cells, reducing the likelihood of developing resistance because targets are more stably expressed. (Sapra et al., 2005)

The first step in designing vascular-targeted nanovectors is to select the most appropriate target ligand-receptor pair for the downstream application. Ideal targets are expressed on the endothelial cell surface in high numbers and homogenously across the cell population at an accessible location in the vasculature. (Sapra and Allen, 2003; Ozawa et al., 2008) The receptor should be inaccessible or expressed in low numbers on non-target tissues. There have been reports that worked out threshold receptor-densities for achieving improvement of therapeutic efficacy for drug-loaded liposomes targeted to cancer-cells. For doxorubicin liposomes targeted with anti-HER2 antibodies, a density of $>10^5$ Her2-receptors on the cancer-cell surface was needed to improve efficacy against an experimental model of metastatic breast cancer. (Park et al., 2002) Similar receptor thresholds have been found for GAH- and CD19-targeted cancer-therapies (Lopes de Menezes et al., 1998; Hosokawa et al., 2003). Another consideration is the choice between internalizing versus non-internalizing receptors. Depending on the application of the NanoSystem it could be necessary for the ligand/receptor pair to internalize after the binding event. For delivery of certain therapeutic modalities intracellular delivery is a must (e.g. plasmid DNA or RNAi).

Whole antibodies, antibody fragments, natural receptor ligands (recombinant or purified), aptamers and low molecular weight ligands such as carbohydrates and peptides or analogues have been used for active targeting strategies (Allen et al., 2002; Hajitou et al., 2006; Levy-Nissenbaum et al., 2008). The challenge is to identify ligands that have a sufficiently high affinity for their targets. This is even more important when using natural receptor ligands as a targeting moiety, since such a ligand will not only have to recognize and bind to the

targeted receptor, but it will also have to compete with the endogenous protein binding to the same receptor-site (Vyas and Sihorkar, 2000). Depending on the downstream application, stability in the circulation is an important parameter also. For drug-delivery applications longer circulation times are desirable to maximize therapeutic effects. For imaging-studies using imaging probes with a short half-life short circulation times are of benefit (e.g. Positron Emission Tomography (PET) imaging with 18F as a positron emitter).

Receptors on endothelial cells, which have been targeted in the past, include receptors for angiogenic proteins, adhesion molecules, metabolic receptors and extracellular matrix components. Numerous studies report the incorporation of targeting moieties into nanoparticles and those of particular interest are summarized below. Emphasis is given to studies which have demonstrated targeting activity in vivo. Among the most widely used vascular targeting agents are peptides containing the arginine-glycine-aspartic acid (RGD) motif directed to the adhesion molecule $\alpha_v\beta_3$-integrin (Pasqualini et al., 1995; Pasqualini et al., 1997). This tri-peptide and analogues have been used extensively for numerous applications, including drug- and gene-delivery and molecular imaging (reviewed in (Temming et al., 2005)). A particularly successful application of this targeting ligand is described by Hood and colleagues (Hood et al., 2002) who used the ligand to target a cationic polymerized lipid-based nanoparticle mixed with a plasmid encoding for the Raf-gene to the tumor vasculature in mice. Pronounced tumor regressions could be achieved after systemic delivery of the gene. Tumor regression could be completely inhibited by pre-blocking the binding sites with free RGD-peptide, showing specificity. (Hood et al., 2002)

Although the notion that a stretch of only three amino acids would serve as such a successful targeting agent was unexpected, there have been more examples of such high-specificity interactions based on short peptide-sequences since. One further example is the NGR-peptide targeting the extracellular matrix component CD13 (Pasqualini et al., 2000). Pastorino et al. used the peptide to target doxorubicin liposomes to tumor-vasculature with anti-vascular effects in models of lung- and ovarian cancer (Pastorino et al., 2006). Interestingly, when this vascular directed treatment was combined with a tumor-targeted therapy (disialoganglioside receptor targeted immunoliposomes), dramatic improvements in the treatment of an animal model of aggressive metastatic neuroblastoma was found. Other extracellular matrix components which have been targeted are aminopeptidase A (Marchio et al., 2004), ICAM-1 and P-selectin. In one study of interest, ICAM-1 targeted polystyrene particles were used to investigate the influence of size and shape on the particle biodistribution in mice. Carrier geometry was found to influence homing in the vasculature, and the rate of endocytosis and lysosomal transport within ECs. Disks had longer half-lives in circulation and higher targeting specificity in mice, whereas spheres were endocytosed more rapidly. Micron-size carriers had prolonged residency in prelysosomal compartments. Submicron carriers trafficked to lysosomes more readily. Therefore, rational design of carrier geometry will help optimize endothelium-targeted therapeutics and may improve efficacy of enzyme replacement therapy for lysosomal disorders. (Muro et al., 2008)
Another study used anti-P-selectin-conjugated liposomes containing VEGF for the selective targeting to the infarcted heart. After treatment, changes in cardiac function and vasculature were quantified in a rat model of myocardial ischemia (MI). Specific delivery of VEGF to post-MI tissue resulted in significant increase in fractional shortening and improved systolic

function. These functional improvements were accompanied by a 21% increase in the number of anatomical vessels and a 74% increase in the number of perfused vessels in the MI region of treated animals. (Scott et al., 2009)

Another class of receptors which have been widely used for vascular targeting are receptors for angiogenic proteins. One obvious example sparked by the marketing of trastuzumab, an antibody directed against Her2, is the targeting of nanosystems to EGF-receptor. Recently, Park and Yoo conjugated an EGF-fragment (11 amino acid peptide) and doxorubicin (DOX) to a bi-functional PEG-polymer. After mixing the conjugate, free DOX and triethylamine "nano-aggregates" spontaneously formed and showed a higher anti-tumor effect in animals bearing human lung-carcinoma xenografts (Park and Yoo, 2009). In a paper by Diagaradjane et al. EGF targeted fluorescent quantum dots were successfully employed for the noninvasive optical imaging of EGFR expression in human colorectal cancer xenografts in mice (Diagaradjane et al., 2008). Other vascular receptors for angiogenic proteins which can be targeted are VEGF, FGF, TNF and TGF.

A very active field of vascular-targeting research is focused on directing nanosystems to the Blood Brain Barrier (BBB). The use of metabolic receptors such as transferrin-receptor has proven particularly useful for directing nanoparticles to the BBB and even across it. This approach has been pioneered by the William Pardridge's research-group who have published numerous successes using antibodies and antibody-fragments ((Pardridge, 2008) for a recent review). Using a similar approach, targeting the insulin-receptor, the group has shown global gene-expression in a primate brain after intravenous administration of pegylated immunoliposomes. (Zhang et al., 2003)

VI. In vitro assays for Nanovectors' characterization

Parallel plate flow chambers have been used to characterize the behavior of circulating cells, as leukocytes and platelets, and can be effectively used to characterize the margination, adhesive and internalization performances of micro/nanoparticles in-vitro. For instance, Decuzzi and colleagues (Gentile et al., 2008a; Decuzzi et al., 2007; Gentile et al., 2008b) have analyzed the non-specific adhesion of spherical fluorescent beads (from 50 nm up to 10 μm) to a cellular layer grown on the chamber substrate under flow.

The apparatus, sketched in Fig. 8, is composed of (i) parallel plate flow chamber, (ii) up-right fluorescent confocal microscope, (iii) digital camera; (iv) pumping system; (v) connecting tubing; (vi) PC and (vii) cellular layer. By decorating the nanovector with fluorescent molecules, the transport along the chamber and the adhesive dynamics to the bottom cell layer can be analyzed over time. An external pumping system (syringe pump) can be connected to the chip through tubings and by changing the pump infusion rate, the mean fluid velocity within the chamber can be changed accordingly. The chamber is rectangular with a length of 20 mm, a width that can be changed from 2.5 mm up to 10 mm and a thickness of 100 μm and 250 μm. However the flow deck can be customized changing the actual geometry of the chamber. By changing the chamber size and the pump infusion rate, the shear stress at the wall can range from zero to few hundreds of Pa, reproducing different hydrodynamic conditions which are physiologically relevant. Through the digital

camera, pictures within the ROI of the moving and stationary particles can be taken at a video rate frequency (> 30 frame per sec) and analyzed offline. From imaging analysis, (i) the surface density of adherent nanovectors ; and (ii) the rate of adhesion and decohesion over time can be measured and compared with the mathematical predictions. Images from a typical flow chamber experiment are given in Fig. 9, showing, from left to right, fluorescent beads adhering to the cellular layer in bright and fluorescent field, imaging analysis and the final result with the variation of the number of beads adhering to the cell layer within the ROI. The same chamber can be heated up to 37°C or cooled down to 4°C to perform internalization experiments over time under flow or in a quiescent medium. Any type of cell growing adherent on a substrate can be used within the flow chamber apparatus.

VII. Intravital Video Microscopy

Quantitative assessment of microvascular phenomena in real-time, *in vivo*, is feasible using intravital microscopy (IVM). A wide variety of microvascular beds are suitable for IVM, both in tissues *in situ* as well as surgically exteriorized vascular beds. The experimental techniques involved vary according to the animal species and vascular bed utilized, details are described in representative publications (Li et al., 2007; Rumbaut et al., 2004; Harris et al., 2002). Commonly these involve anesthesia followed by instrumentation to monitor and maintain the animal's physiologic state and enable administration of exogenous substances (e.g., arterial, venous, tracheal catheters, temperature probes, homeothermic systems, etc). Fig. 10 provides examples of three microvascular beds: cremaster muscle, mesentery, and the limbal vessels surrounding the cornea. As evident in the figure, the optical characteristics of thin tissues like the cremaster and mesentery (panels A & B) enable brightfield observations of the interactions between blood cells and microvascular endothelium. In contrast, imaging of thicker tissues such as the limbal vessels of the cornea is typically performed with epifluorescence microscopy (panel C).

Quantitative data generated with these techniques include measures of network architecture, vascular diameters, flow patterns, mean blood velocity, and interactions between blood cells and endothelial cells (Li et al., 2006; Rumbaut et al., 2005), among many others. IVM is also used to allow *in situ*, *in vivo*, single microvessel perfusion, for example, to measure microvascular pressures, hydraulic conductivity or macromolecular permeability (Rumbaut et al., 2000; Rumbaut and Huxley, 2002), as well as for electrophysiologic studies of microvascular endothelial and smooth muscle cells (Welsh et al., 1998).

IVM has also been used to monitor the dynamics of micro- and nano-particles in the microcirculation, and their interactions with blood cells and endothelial cells (Ravnic et al., 2007; Smith et al., 2003). These studies involve epifluorescence microscopy, since the spatial resolution of brightfield systems is typically insufficient to resolve particles in vivo. Using low-intensity epi-illumination (to minimize light/dye-induced phototoxicity and photobleaching) and high-sensitivity imaging, the kinetics of individual fluorescently-labeled particles may be resolved reliably, as depicted in Fig. 11.

Further, combining this approach with flash epi-illumination has been used to estimate fluid velocity profiles in the plasma region near the vessel wall (Smith et al., 2003). These studies

reveal the presence of a hydrodynamically significant layer on the surface of endothelial cells, of comparable thickness to those obtained using other IVM-based optical approaches to estimate the thickness of the glycocalyx *in vivo* (~0.5 μm, ref. (Vink and Duling, 1996)).

The suitability of specific nanoparticulate systems for intravital microscopy depends on various physicochemical properties of the particles (Ravnic et al., 2007), such as size, surface charge and fluorescence intensity. Further, the signal-to-noise ratio for individual applications is impacted by the sensitivity of the imaging system, and a variety of biological parameters, which vary according to the vascular bed. These include tissue autofluorescence, and motion artifacts of various frequencies, induced from respiratory excursions, peristalsis, heart beat, muscle contraction. Despite these limitations, intravital microscopy is a powerful tool to assess the in vivo kinetics of nanoparticles, including their interactions with blood cells and endothelial cells *in vivo*. These techniques represent a significant component of an integrated approach for the rational design of nanoparticulate systems for biological imaging and therapy.

VIII. Conclusions

The presented integrated approach combines multi-scale/multi-physics mathematical models (Math Tools) with in-vitro assays (In-vitro Apparatus) and in-vivo intravital microscopy experiments (IntraVital Microscopy). By doing so, it aims at identifying the optimal combination of size, shape and surface properties that maximize the nanovectors localization within the diseased microvasculature. The integration among the three fundamental components and the flow of data and information is shown schematically in Fig. 12. The geometry of the vascular network, its permeability to plasma, molecules and nanovectors, and the hemodynamic conditions can be estimated in the authentic vasculature of small animals, as described in Intravital Video Microscopy paragraph VII, and the adhesive properties of the nanovectors (association and dissociation coefficients) can be measured using flow chamber systems, as shown in paragraph VI. These data can be used to accurately define the boundary and initial conditions for the transport, adhesion and internalization problem presented in paragraph II. The results of the mathematical models, in terms of number density of nanovectors adhering to the diseased vasculature; and the volume concentration of circulating and extravasated nanovectors can be readily compared with the in-vitro and in-vivo experimental results to validate the models and further refine the models and parameters used. Such an approach not only helps in identifying the best size, shape and surface properties combination for a specific nanovector, but it could also dramatically reduce the time and costs for developing and optimize new nanovectors for biomedical applications.

Acknowledgments

This work has been partially supported by the Telemedicine and Advanced Technology Research Center (TATRC) of the U.S.Army Medical Research Acquisition Activity (USAMRAA) through the pre-Center Grant entitled “Rational Design of Particulate Systems for the Imaging and Hyperthermia Treatment of an Inflamed Endothelium”.

References

1. Adams GP, Schier R, McCall AM, Simmons HH, Horak EM, Alpaugh RK, Marks JD, Weiner LM. High affinity restricts the localization and tumor penetration of single-chain fv antibody molecules. Cancer Res. 2001; 61:4750. [PubMed: 11406547]
2. Allen TM. Ligand-targeted therapeutics in anticancer therapy Nat. Rev Drug Discov. 2002; 2:750.
3. Allen TM. Ligand-targeted therapeutics in anticancer therapy. Nat Rev Drug Discov. 2002; 2:750.
4. Allen TM, Ahmad I, Lopes de Menezes DE, Moase EH. Immunoliposome-mediated targeting of anti-cancer drugs in vivo. Biochem Soc Trans. 1995; 23:1073–1079. [PubMed: 8654684]
5. Allen TM, Sapra P, Moase E, Moreira J, Iden D. Adventures in targeting. J Liposome Res. 2002; 12:5–12. [PubMed: 12604033]
6. Amiji, MM. Nanotechnology for cancer therapy. CRC press; 2007. p. 258-260.
7. Andersson L, Davies J, Duncan R, Ferruti P, Ford J, Kneller S, Mendichi R, Pasut G, Schiavon O, Summerford C, Tirk A, Veronese FM, Vincenzi V, Wu G. Poly(ethylene glycol)-poly(ester-carbonate) block copolymers carrying PEG-peptidyl-doxorubicin pendant side chains: synthesis and evaluation as anticancer conjugates. Biomacromolecules. 2005; 6:914–926. [PubMed: 15762660]
8. Banerjee RK, van Osdol W, Bungay PM, Sung C, Dedrick RL. Finite element model of antibody penetration in a prevascular tumor nodule embedded in normal tissue. J Control Release. 2001; 74:193. [PubMed: 11489495]
9. Barth, HG. Modern methods of particle size analysis. Vol. 73. Wiley-Interscience; 1984.
10. Brannon-Peppas L, Blanchette JO. Nanoparticle and targeted systems for cancer therapy. Adv Drug Deliver Rev. 2004; 56:1649.
11. Champion JA, Mitragotri S. Role of Target Geometry in Phagocytosis. Proc Natl Acad Sci USA. 2006; 103:4930–4. [PubMed: 16549762]
12. Decuzzi P, Ferrari M. The adhesive strength of non-spherical particles mediated by specific interactions. Biomaterials. 2006; 27:5307–14. [PubMed: 16797691]
13. Decuzzi P, Ferrari M. The role of specific and non-specific interactions in receptor-mediated endocytosis of nanoparticles. Biomaterials. 2007; 28:2915–22. [PubMed: 17363051]
14. Decuzzi P, Ferrari M. Design maps for nanoparticles targeting the diseased microvasculature. Biomaterials. 2008; 29:377–84. [PubMed: 17936897]
15. Decuzzi P, Gentile F, Granaldi A, Curcio A, Causa F, Indolfi C, Netti P, Ferrari M. Flow Chamber Analysis of Size Effects in the Adhesion of Spherical Particles. Int J Nanomed. 2007; 2:689–96.
16. Decuzzi P, Lee S, Bhushan B, Ferrari M. A theoretical model for the margination of particles within blood vessels. Ann Biomed Eng. 2005; 33:179–90. [PubMed: 15771271]
17. Decuzzi P, Lee S, Decuzzi M, Ferrari M. Adhesion of microfabricated particles on vascular endothelium: a parametric analysis. Ann Biomed Eng. 2004; 32:793–802. [PubMed: 15255210]
18. Decuzzi P, Pasqualini R, Arap W, Ferrari M. Intravascular delivery of particulate systems: does geometry really matter? Pharm Res. 2009; 2009:26235–43.
19. Diagaradjane P, Orenstein-Cardona JM, Colon-Casasnovas NE, Deorukhkar A, Shentu S, Kuno N, Schwartz DL, Gelovani JG, Krishnan S. Imaging epidermal growth factor receptor expression in vivo: pharmacokinetic and biodistribution characterization of a bioconjugated quantum dot nanoprobe. Clin Cancer Res. 2008; 14:731–741. [PubMed: 18245533]
20. Donaldson, K.; Borm, P. Particle Toxicology. CRC Press; 2007. p. 49-56.
21. Douziech-Eyrolles L, Marchais H, Herve K, Munnier E, Souce M, Linassier C, Dubois P, Chourpa I. Nanovectors for anticancer agents based on superparamagnetic iron oxide nanoparticles. Int J Nanomed. 2007; 2:541.
22. Drummond DC, Meyer O, Hong K, Kirpotin DB, Papahadjopoulos D. Optimizing liposomes for delivery of chemotherapeutic agents to solid tumors. Pharmacol Rev. 1999; 51:691. [PubMed: 10581328]
23. Duncan R. The dawning era of polymer therapeutics. Nat Rev Drug Discov. 2003; 2:347. [PubMed: 12750738]
24. Duncan R. Polymer conjugates as anticancer nanomedicines. Nat Rev Cancer. 2006; 6:688. [PubMed: 16900224]

25. Farokhzad OC, Cheng J, Teply BA, Sherifi I, Jon S, Kantoff PW, Richie JP, Langer R. Targeted nanoparticle-aptamer bioconjugates for cancer chemotherapy in vivo. Proc Natl Acad Sci USA. 2006a; 103:6315. [PubMed: 16606824]
26. Farokhzad OC, Karp JM, Langer R. Nanoparticle-aptamer bioconjugates for cancer targeting. Expert Opin Drug Deliver. 2006b; 3:311.
27. Ferrari M. Cancer nanotechnology: opportunities and challenges. Nat Rev Cancer. 2005; 5:161–71. [PubMed: 15738981]
28. Ferrari M. Nanovector therapeutics. Curr Opin Chem Biol. 2005; 9:343. [PubMed: 15967706]
29. Ferrari M. Nanovector therapeutics. Curr Opin Chem Biol. 2005; 9:343. [PubMed: 15967706]
30. Ferrari M. Nanogeometry: beyond drug delivery Nat. Nanotech. 2008; 3:131.
31. From VASCULAR TARGETING MOITIES
32. Fung, YC. Biomechanics: Mechanical Properties of Living Tissues. Springer; 1993.
33. Gentile F, Chiappini C, Fine D, Bhavane RC, Peluccio MS, Cheng MM, Liu X, Ferrari M, Decuzzi P. The effect of shape on the margination dynamics of non-neutrally buoyant particles in two-dimensional shear flows. J Biomech. 2008b; 41:2312–8. [PubMed: 18571181]
34. Gentile F, Curcio A, Indolfi C, Ferrari M, Decuzzi P. The margination propensity of spherical particles for vascular targeting in the microcirculation. J Nanobiotech. 2008a; 6:9.
35. Goldman AJR, Cox G, Brenner H. Slow viscous motion of a sphere parallel to a plane wall., II., Couette flow. Chem Eng Sci. 1967; 22:635– 660.
36. Goldsmith HL, Spain S. Margination of leukocytes in blood flow through small tubes. Microvasc Res. 1984; 27:204–22. [PubMed: 6708830]
37. Goren D, Horowitz AT, Zalipsky S, Woodle MC, Yarden Y, Gabizon A. Targeting of stealth liposomes to erbB-2 (Her/2) receptor: in vitro and in vivo studies. Br J Cancer. 1996; 74:1749. [PubMed: 8956788]
38. Gotoh, K.; Masuda, H.; Higashitani, K. Powder technology handbook. Marcel Dekker; 1997. p. 43-55.
39. Gradishar WJ, Tjulandin S, Davidson N, Shaw H, Desai N, Bhar P, Hawkins M, O'Shaughnessy J. Phase III trial of nanoparticle albumin-bound paclitaxel compared with polyethylated castor oil-based paclitaxel in women with breast cancer. J Clin Oncol. 2005; 23:7794. [PubMed: 16172456]
40. Hajitou A, Pasqualini R, Arap W. Vascular targeting: recent advances and therapeutic perspectives. Trends Cardiovasc Med. 2006; 16:80–88. [PubMed: 16546688]
41. Hajitou A, Trepel M, Lilley CE, Soghomonyan S, Alauddin MM, Marini FC 3rd, Restel BH, Ozawa MG, Moya CA, Rangel R, Sun Y, Zaoui K, Schmidt M, von Kalle C, Weitzman MD, Gelovani JG, Pasqualini R, Arap W. A hybrid vector for ligand-directed tumor targeting and molecular imaging. Cell. 2006; 125:385. [PubMed: 16630824]
42. Harris JM, Chess RB. Effect of pegylation on pharmaceuticals. Nat Rev Drug Discov. 2003; 2:214. [PubMed: 12612647]
43. Harris NR, Whitt SP, Zilberberg J, Alexander JS, Rumbaut RE. Extravascular transport of fluorescently labeled albumins in the rat mesentery. Microcirculation. 2002; 9:177–187. [PubMed: 12080415]
44. Heath JR, Davis ME. Nanotechnology and cancer. Annu Rev Med. 2008; 59:251. [PubMed: 17937588]
45. Herant M, Heinrich V, Dembo M. Mechanics of neutrophil phagocytosis: experiments and quantitative models. J Cell Sci. 2006; 119:1903–1913. [PubMed: 16636075]
46. Hirsch LR, Stafford RJ, Bankson JA, Sershen SR, Rivera B, Price RE, Hazle JD, Halas NJ, West JL. Nanoshell-mediated near-infrared thermal therapy of tumors under magnetic resonance guidance. Proc Natl Acad Sci USA. 2003; 100:13549. [PubMed: 14597719]
47. Hofheinz RD, Gnad-Vogt SU, Beyer U, Hochhaus A. Liposomal encapsulated anti-cancer drugs. Anti-Cancer Drugs. 2005; 16:691. [PubMed: 16027517]
48. Hood JD, Bednarski M, Frausto R, Guccione S, Reisfeld RA, Xiang R, Cheresh DA. Tumor regression by targeted gene delivery to the neovasculature. Science. 2002; 296:2404–2407. [PubMed: 12089446]

49. Hosokawa S, Tagawa T, Niki H, Hirakawa Y, Nohga K, Nagaike K. Efficacy of immunoliposomes on cancer models in a cell-surface-antigen-density- dependent manner. Br J Cancer. 2003; 89:1545–1551. [PubMed: 14562030]
50. Jain RK. Transport of molecules across tumor vasculature. Cancer Metastasis Rev. 1987; 6:559–594. [PubMed: 3327633]
51. Jain RK. Transport of molecules, particles, and cells in solid tumors. Annu Rev Biomed Eng. 1999; 1:241–63. [PubMed: 11701489]
52. Jain RK, Baxter LT. Mechanisms of heterogeneous distribution of monoclonal antibodies and other macromolecules in tumors: significance of elevated interstitial pressure. Cancer Res. 1988; 48:7022–32. [PubMed: 3191477]
53. Jiang W, Kim BY, Rutka JT, Chan WC. Nanoparticle-mediated cellular response is size-dependent. Nat Nanotechnol. 2008; 3:145–50. [PubMed: 18654486]
54. Juweid M, Neumann R, Paik C, Perez-Bacete MJ, Sato J, van Osdol W, Weinstein JN. Micropharmacology of monoclonal antibodies in solid tumors: direct experimental evidence for a binding site barrier. Cancer Res. 1992; 52:5144. [PubMed: 1327501]
55. Kang J, Lee MS, Copland JAIII, Luxon BA, Gorenstein DG. Combinatorial selection of a single stranded DNA thioaptamer targeting TGF-beta1 protein. Bioorg Med Chem Lett. 2008; 18:1835. [PubMed: 18294846]
56. Kim S, Kong RL, Popel AS, Intaglietta M, Johnson PC. Temporal and spatial variations of cell-free layer width in arterioles. Am J Physiol Heart Circ Physiol. 2007; 293:H1526–H1535. [PubMed: 17526647]
57. Klibanov AL, Maruyama K, Beckerleg AM, Torchilin VP, Huang L. Activity of amphipathic poly(ethylene glycol) 5000 to prolong the circulation time of liposomes depends on the liposome size and is unfavorable for immunoliposome binding to target. Biochim Biophys Acta. 1991; 1062:142. [PubMed: 2004104]
58. Korgel BA, Zanten JH, Monbouquette HG. Vesicle Size Distributions measured by Flow Field-Flow Fractionation Coupled with Multiangle Light Scattering. Biophys J. 1998; 74:3264–3272. [PubMed: 9635780]
59. Koval M, Preiter K, Adles C, Stahl PD, Steinberg TH. Size of IgG- Opsonized Particles Determines Macrophage Response during Internalization. Experimental Cell Res. 1998; 242:265–273.
60. Langer R. Drug delivery and targeting. Nature. 1998; 392:5. [PubMed: 9579855]
61. Lee SY, Ferrari M, Decuzzi P. Design of bio-mimetic particles with enhanced vascular interaction. J Biomech. 2009; 42(12):1885–90. [PubMed: 19523635]
62. Leung DW, Cachianes G, Kuang WJ, Goeddel DV, Ferrara N. Vascular endothelial growth factor is a secreted angiogenic mitogen. Science. 1989; 246:1306–1309. [PubMed: 2479986]
63. Levy-Nissenbaum E, Radovic-Moreno AF, Wang AZ, Langer R, Farokhzad OC. Nanotechnology and aptamers: applications in drug delivery. Trends Biotechnol. 2008; 26:442–449. [PubMed: 18571753]
64. Li Z, Burns AR, Rumbaut RE, Smith CW. g/d T Cells Are Necessary for Platelet and Neutrophil Accumulation in Limbal Vessels and Efficient Epithelial Repair after Corneal Abrasion. Am J Pathol. 2007; 171:838–845. [PubMed: 17675580]
65. Li Z, Rumbaut RE, Burns AR, Smith CW. Platelet response to corneal abrasion is necessary for acute inflammation and efficient re-epithelialization. Invest Ophthalmol Vis Sci. 2006; 47:4794–4802. [PubMed: 17065490]
66. Lopes de Menezes DE, Pilarski LM, Allen TM. In vitro and in vivo targeting of immunoliposomal doxorubicin to human B-cell lymphoma. Cancer Res. 1998; 58:3320–3330. [PubMed: 9699662]
67. Maeda H, Fang J, Inutsuka T, Kitamoto Y. Vascular permeability enhancement in solid tumor: various factors, mechanisms involved and its implications. Int Immunopharmacol. 2003; 3:319–328. [PubMed: 12639809]
68. Maeda H, Noguchi Y, Sato K, Akaike T. Enhanced vascular permeability in solid tumor is mediated by nitric oxide and inhibited by both new nitric oxide scavenger and nitric oxide synthase inhibitor. Jpn J Cancer Res. 1994; 85:331–334. [PubMed: 7515384]

69. Maeda H, Wu J, Sawa T, Matsumura Y, Hori K. Tumor vascular permeability and the EPR effect in macromolecular therapeutics: a review. J Control Release. 2000; 65:271. [PubMed: 10699287]
70. Maeda H, Wu J, Sawa T, Matsumura Y, Hori K. Tumor vascular permeability and the EPR effect in macromolecular therapeutics: a review. J Control Release. 2000; 65:271. [PubMed: 10699287]
71. Marchio S, Lahdenranta J, Schlingemann RO, Valdembri D, Wesseling P, Arap MA, Hajitou A, Ozawa MG, Trepel M, Giordano RJ, Nanus DM, Dijkman HB, Oosterwijk E, Sidman RL, Cooper MD, Bussolino F, Pasqualini R, Arap W. Aminopeptidase A is a functional target in angiogenic blood vessels. Cancer cell. 2004; 5:151–162. [PubMed: 14998491]
72. Mohammed AR, Weston N, Coombes AG, Fitzgerald M, Perrie Y. Liposome formulation of poorly water soluble drugs: optimisation of drug loading and ESEM analysis of stability. Int J Pharm. 2004; 285(1–2):23–34. [PubMed: 15488676]
73. Monsky WL, Kruskal JB, Lukyanov AN, Girnun GD, Ahmed M, Gazelle GS, Huertas JC, Stuart KE, Torchilin VP, Goldberg SN. Radio-frequency ablation increases intratumoral liposomal doxorubicin accumulation in a rat breast tumor model. Radiology. 2002; 224:823. [PubMed: 12202721]
74. Muro S, Garnacho C, Champion JA, Leferovich J, Gajewski C, Schuchman EH, Mitragotri S, Muzykantov VR. Control of endothelial targeting and intracellular delivery of therapeutic enzymes by modulating the size and shape of ICAM-1-targeted carriers. Mol Ther. 2008; 16:1450–1458. [PubMed: 18560419]
75. Neofytou P. Comparison of blood rheological models for physiological flow simulation. Biorheology. 2004; 41(6):693–714. [PubMed: 15851845]
76. Neri D, Bicknell R. Tumour vascular targeting. Nat Rev Cancer. 2005; 5:436–46. [PubMed: 15928674]
77. Nie S, Kim GJ, Xing Y, Simons JW. Nanotechnology applications in cancer. Annu Rev Biomed Eng. 2007; 9:257. [PubMed: 17439359]
78. Ozawa MG, Zurita AJ, Dias-Neto E, Nunes DN, Sidman RL, Gelovani JG, Arap W, Pasqualini R. Beyond receptor expression levels: the relevance of target accessibility in ligand-directed pharmacodelivery systems. Trends Cardiovasc Med. 2008; 18:126–132. [PubMed: 18555185]
79. Pardridge WM. Re-engineering biopharmaceuticals for delivery to brain with molecular Trojan horses. Bioconjug Chem. 2008; 19:1327–1338. [PubMed: 18547095]
80. Park JW, Hong K, Kirpotin DB, Colbern G, Shalaby R, Baselga J, Shao Y, Nielsen UB, Marks JD, Moore D, Papahadjopoulos D, Benz CC. Anti-HER2 immunoliposomes: enhanced efficacy attributable to targeted delivery. Clin Cancer Res. 2002; 8:1172–1181. [PubMed: 11948130]
81. Park S, Yoo HS. In vivo and in vitro anti-cancer activities and enhanced cellular uptakes of EGF fragment decorated doxorubicin nano-aggregates. Int J Pharm. 2009
82. Parveen S, Sahoo SK. Nanomedicine: clinical applications of polyethylene glycol conjugated proteins and drugs. Clin Pharmacokinet. 2006; 45:965. [PubMed: 16984211]
83. Pasqualini R, Koivunen E, Ruoslahti E. A peptide isolated from phage display libraries is a structural and functional mimic of an RGD-binding site on integrins. J Cell Biol. 1995; 130:1189–1196. [PubMed: 7657703]
84. Pasqualini R, Koivunen E, Ruoslahti E. Alpha v integrins as receptors for tumor targeting by circulating ligands. Nat Biotechnol. 1997; 15:542–546. [PubMed: 9181576]
85. Pasqualini R, Koivunen E, Kain R, Lahdenranta J, Sakamoto M, Stryhn A, Ashmun RA, Shapiro LH, Arap W, Ruoslahti E. Aminopeptidase N is a receptor for tumor-homing peptides and a target for inhibiting angiogenesis. Cancer Res. 2000; 60:722–727. [PubMed: 10676659]
86. Pastorino F, Brignole C, Di Paolo D, Nico B, Pezzolo A, Marimpietri D, Pagnan G, Piccardi F, Cilli M, Longhi R, Ribatti D, Corti A, Allen TM, Ponzoni M. Targeting liposomal chemotherapy via both tumor cell-specific and tumor vasculature-specific ligands potentiates therapeutic efficacy. Cancer Res. 2006; 66:10073–10082. [PubMed: 17047071]
87. Peer D, Karp JM, Hong SY, Farokhzad O, Margalit R, Langer R. Nanocarriers as an emerging platform for cancer therapy. Nat Nanotech. 2007; 2:751.
88. Peltonen L, Hirvonen J. Physicochemical characterisation of Nano- and Microparticles. Curr Nanosci. 2008; 4(1):101–107.

89. Philippot, JR.; Schuber, F. Liposomes as Tolls in Basic research and industry. CRC press; Boca Raton, FL: 1995.
90. Ravnic DJ, Zhang YZ, Turhan A, Tsuda A, Pratt JP, Huss HT, Mentzer SJ. Biological and optical properties of fluorescent nanoparticles developed for intravascular imaging. Microsc Res Tech. 2007; 70:776–781. [PubMed: 17576122]
91. Rejman J, Oberlem V, Zuhorn IS, Hoekstra D. Size-dependent internalization of particles via the pathways of clathrin- and caveolae-mediated endocytosis. Biochem J. 2004; 377:159–169. [PubMed: 14505488]
92. Riehemann K, Schneider SW, Luger TA, Godin B, Ferrari M, Fuchs H. Nanomedicine - Developments and perspectives. Angewandte Chemie - International Edition. 2008; 48:872–897.
93. Ringsdorf H. Structure and properties of pharmacologically active polymers. J Polym Sci. 1975; 51:135.
94. Rumbaut RE, Huxley VH. Similar permeability responses to nitric oxide synthase inhibitors of venules from three animal species. Microvasc Res. 2002; 64:21–31. [PubMed: 12074627]
95. Rumbaut RE, Randhawa JK, Smith CW, Burns AR. Mouse cremaster venules are predisposed to light/dye-induced thrombosis independent of wall shear rate. CD18 ICAM-1 or P-selectin. Microcirculation. 2004; 11:239–247. [PubMed: 15280078]
96. Rumbaut RE, Slaaf DW, Burns AR. Microvascular thrombosis models in venules and arterioles in vivo. Microcirculation. 2005; 12:259–274. [PubMed: 15814435]
97. Rumbaut RE, Wang J, Huxley VH. Differential effects of L-NAME on rat venular hydraulic conductivity. Am J Physiol Heart Circ Physiol. 2000; 279:H2017–H2023. [PubMed: 11009493]
98. Ruozi B, Tosi G, Forni F, Fresta M, Vandelli MA. Atomic force microscopy and photon correlation spectroscopy: two techniques for rapid characterization of liposomes. Eur J Pharm Sci. 2005; 25(1):81–9. [PubMed: 15854804]
99. Sakamoto J, Annapragada A, Decuzzi P, Ferrari M. Antibiological barrier nanovector technology for cancer applications. Expert Opin Drug Deliver. 2007; 4:359.
100. Sanhai WR, Sakamoto JH, Canady R, Ferrari M. Seven challenges for nanomedicine. Nat Nanotech. 2008; 3:242.
101. Sapra P, Allen TM. Ligand-targeted liposomal anticancer drugs. Prog Lipid Res. 2003; 42:439–462. [PubMed: 12814645]
102. Sapra P, Tyagi P, Allen TM. Ligand-targeted liposomes for cancer treatment. Curr Drug Deliv. 2005; 2:369–381. [PubMed: 16305440]
103. Saul JM, Annapragada AV, Bellamkonda RV. A dual-ligand approach for enhancing targeting selectivity of therapeutic nanocarriers. J Control Release. 2006; 114:277. [PubMed: 16904220]
104. Schroeder A, Avnir Y, Weisman S, Najajreh Y, Gabizon A, Talmon Y, Kost J, Barenholz Y. Controlling liposomal drug release with low frequency ultrasound: mechanism and feasibility. Langmuir. 2007; 23:4019. [PubMed: 17319706]
105. Scott RC, Rosano JM, Ivanov Z, Wang B, Chong PL, Issekutz AC, Crabbe DL, Kiani MF. Targeting VEGF-encapsulated immunoliposomes to MI heart improves vascularity and cardiac function. FASEB J. 2009
106. Senger DR, Galli SJ, Dvorak AM, Perruzzi CA, Harvey VS, Dvorak HF. Tumor cells secrete a vascular permeability factor that promotes accumulation of ascites fluid. Science. 1983; 219:983–985. [PubMed: 6823562]
107. Sengupta S, Eavarone D, Capila I, Zhao G, Watson N, Kiziltepe T, Sasisekharan R. Temporal targeting of tumour cells and neovasculature with a nanoscale delivery system. Nature. 2005; 436:568. [PubMed: 16049491]
108. Sergeeva A, Kolonin MG, Molldrem JJ, Pasqualini R, Arap W. Display technologies: application for the discovery of drug and gene delivery agents. Adv Drug Deliver Rev. 2006; 58:1622–54.
109. Seymour LW. Passive tumor targeting of soluble macromolecules and drug conjugates. Crit Rev Ther Drug Carrier Syst. 1992; 9:135–187. [PubMed: 1386002]
110. Sharan M, Popel AS. A two-phase model for flow of blood in narrow tubes with increased effective viscosity near the wall. Biorheology. 2001; 38:415–28. [PubMed: 12016324]

111. Smith ML, Long DS, Damiano ER, Ley K. Near-wall micro-PIV reveals a hydrodynamically relevant endothelial surface layer in venules in vivo. Biophys J. 2003; 85:637–645. [PubMed: 12829517]
112. Souza GR, Yonel-Gumruk E, Fan D, Easley J, Rangel R, Guzman-Rojas L, Miller JH, Arap W, Pasqualini R. Bottom-up assembly of hydrogels from bacteriophage and Au nanoparticles: the effect of cis- and trans-acting factors. PLoS ONE. 2008; 3:e2242. [PubMed: 18493583]
113. Souza GR, Christianson DR, Staquicini FI, et al. Networks of gold nanoparticles and bacteriophage as biological sensors and cell-targeting agents. Proc Natl Acad Sci USA. 2006; 103:1215. [PubMed: 16434473]
114. Stolnik S, Illum L, Davis SS. Long circulating microparticulate drug carriers. Adv Drug Deliver Rev. 1995; 16:195–214.
115. Tasciotti E, Liu X, Bhavane R, Plant K, Leonard AD, Price BK, Cheng MM, Decuzzi P, Tour JM, Robertson FM, Ferrari M. Mesoporous silicon particles as a multistage delivery system for imaging and therapeutic applications. Nature Nanotechnology. 2008; 3:151.
116. Temming K, Schiffelers RM, Molema G, Kok RJ. RGD-based strategies for selective delivery of therapeutics and imaging agents to the tumour vasculature. Drug Resist Updat. 2005; 8:381–402. [PubMed: 16309948]
117. Torchilin VP. Recent advances with liposomes as pharmaceutical carriers. Nat Rev Drug Discov. 2005; 4:145. [PubMed: 15688077]
118. Torchilin VP. Targeted pharmaceutical nanocarriers for cancer therapy and imaging. The AAPS Journal. 2007; 9:E128. [PubMed: 17614355]
119. Tyle P, Ram BP. Monoclonal antibodies. immunoconjugates. and liposomes as targeted therapeutic systems. Targeted Diagn Ther. 1990; 3:3–22. [PubMed: 2131014]
120. Vasey PA, Kaye SB, Morrison R, Twelves C, Wilson P, Duncan R, Thomson AH, Murray LS, Hilditch TE, Murray T. Phase I clinical and pharmacokinetic study of PK1 [N-(2-hydroxypropyl)methacrylamide copolymer doxorubicin]: first member of a new class of chemotherapeutic agents-drug-polymer conjugates. Cancer Research Campaign Phase I/II Committee. Clin Cancer Res. 1999; 5:83. [PubMed: 9918206]
121. Vink H, Duling BR. Identification of distinct luminal domains for macromolecules. erythrocytes. and leukocytes within mammalian capillaries. Circ Res. 1996; 79:581–589. [PubMed: 8781491]
122. Vyas SP, Sihorkar V. Endogenous carriers and ligands in non-immunogenic site-specific drug delivery. Adv Drug Deliv Rev. 2000; 43:101–164. [PubMed: 10967224]
123. Wang AZ, Gu F, Zhang L, Chan JM, Radovic-Moreno A, Shaikh MR, Farokhzad OC. Biofunctionalized targeted nanoparticles for therapeutic applications. Expert Opin Biol Ther. 2008; 8:1063–70. [PubMed: 18613759]
124. Welsh DG, Jackson WF, Segal SS. Oxygen induces electromechanical coupling in arteriolar smooth muscle cells: a role for L-type Ca2+ channels. Am J Physiol. 1998; 274:H2018–2024. [PubMed: 9841528]
125. Yang X, Wang H, Beasley DW, Volk DE, Zhao X, Luxon BA, Lomas LO, Herzog NK, Aronson JF, Barrett AD, Leary JF, Gorenstein DG. Selection of thioaptamers for diagnostics and therapeutics. Ann NY Acad Sci. 2006; 116:1082.
126. Zhang L, Gu FX, Chan JM, Wang AZ, Langer RS, Farokhzad OC. Nanoparticles in medicine: therapeutic applications and developments. Clin Pharmacol Ther. 2007; 83:761. [PubMed: 17957183]
127. Zhang Y, Schlachetzki F, Pardridge WM. Global non-viral gene transfer to the primate brain following intravenous administration. Mol Ther. 2003; 7:11–18. [PubMed: 12573613]
128. Zuidam, NJ.; de Vruch, R.; Crommelin, DJA. Liposomes. Torchilin, VP.; Weissing, V., editors. Oxford University Press; New York: 2003. p. 31-77.

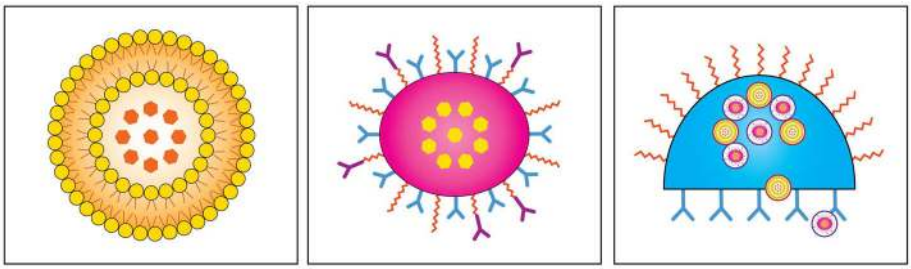

Fig. 1.

(a) First-generation nanovectors, as the currently clinical liposomes, comprise a container (phospholipidic bilayer in yellow) and an active principle (red dots). They localize in the tumor by enhanced permeation and retention (EPR); (b) Second-generation nanovectors further possess the ability for the targeting of their therapeutic action via antibodies and other biomolecules, remote activation, or responsiveness to environment; (c) Third-generation nanovectors such as multistage agents are capable of more complex functions, such a time-controlled deployment of multiple waves of active nanoparticles, deployed across different biological barriers and with different sub-cellular targets.

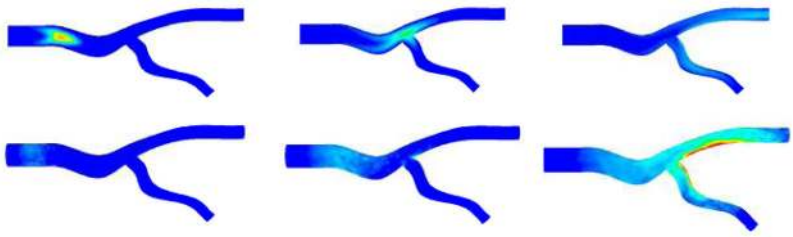

Fig. 2.

Concentration C of nanovectors transported along an authentically complex vascular network (top) and wall concentration C_w (bottom) of nanovectors at t=3, 6 and 9 sec after a bolus injection within the inlet section (from direction from left to right).

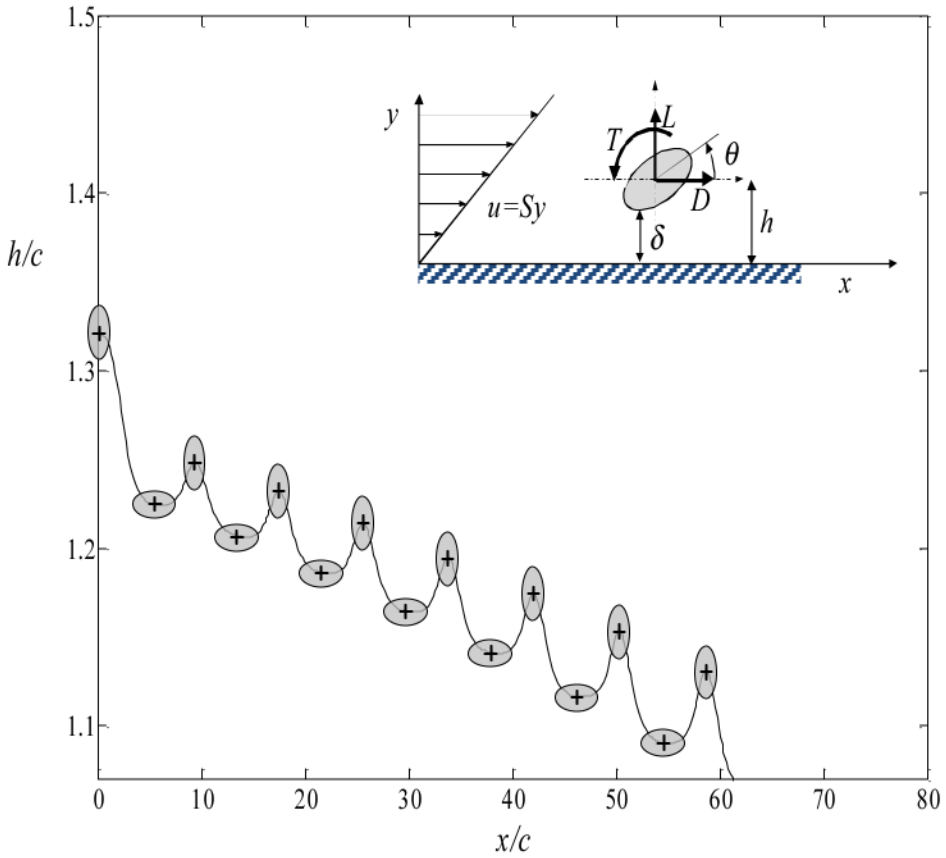

Fig. 3.

The dynamics of an ellipsoidal particle (aspect ratio 0.5) moving in proximity to a vessel wall. The particle is drifting towards the wall at the bottom of the plot [adapted from Lee et al., 2009].

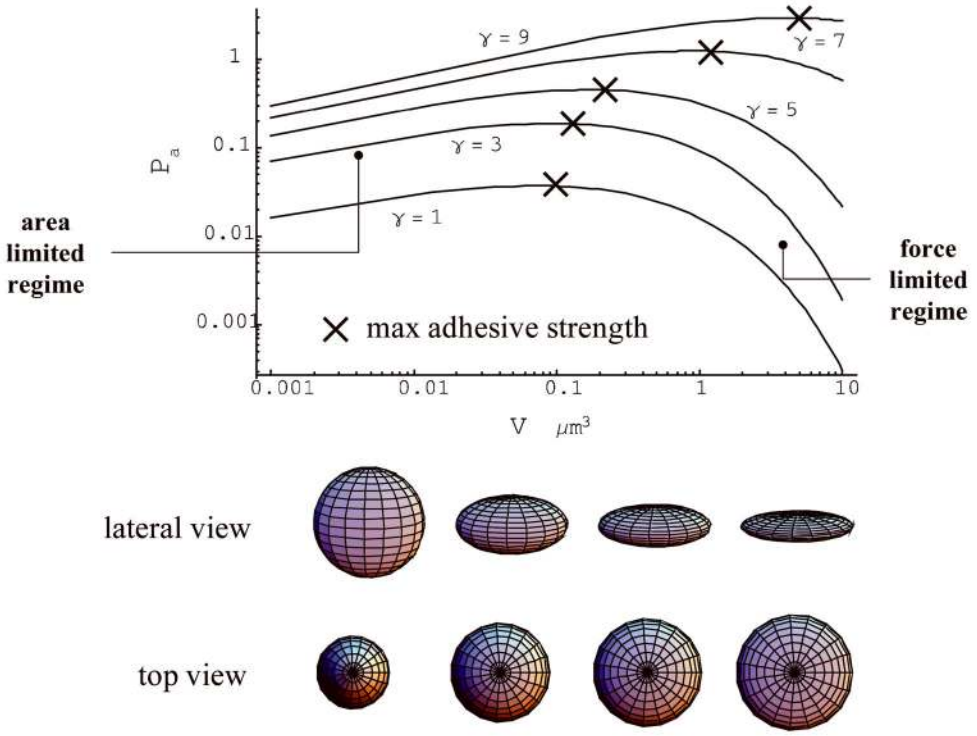

Fig. 4.

The probability of adhesion for a spheroidal particle in a capillary flow [adapted from Decuzzi et al., 2004]

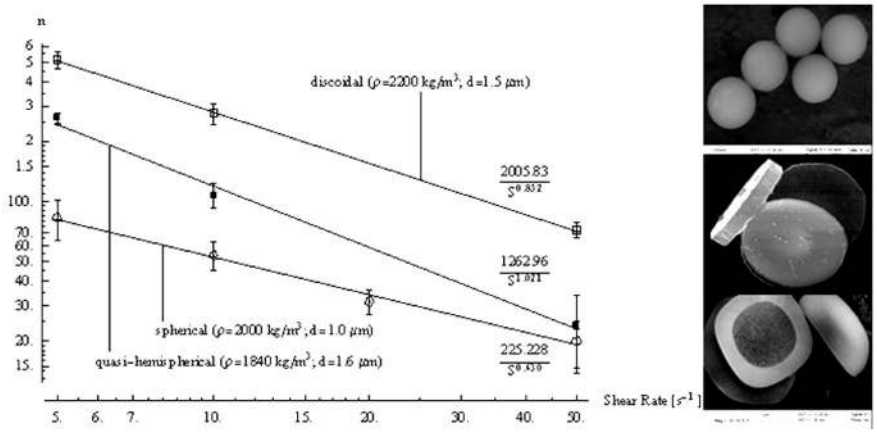

Fig. 5.

Number of marginating nanoparticles as a function of the shear rate and particle shape [adapted from Decuzzi and Ferrari, 2006]

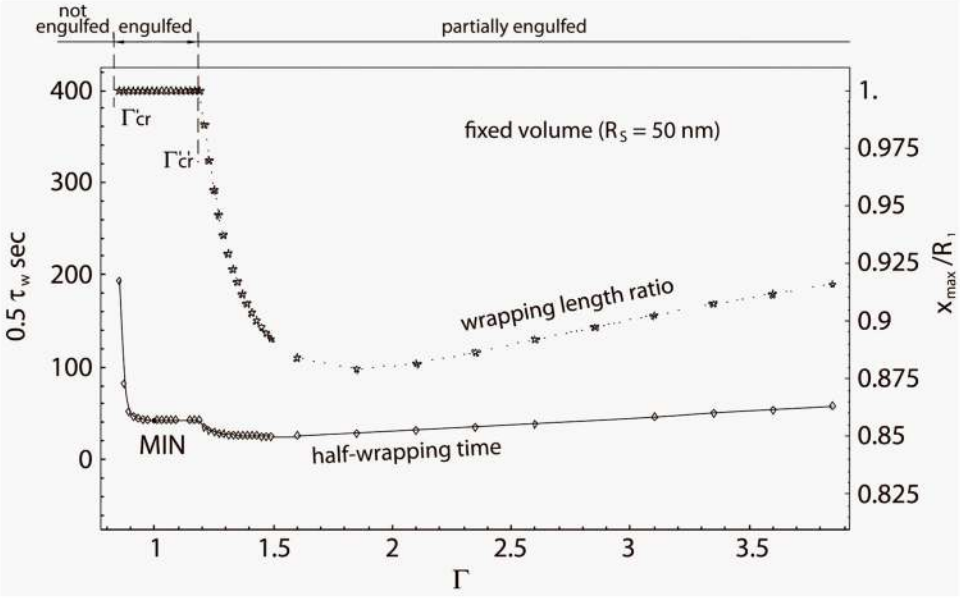

Fig. 6.

Characteristic half-time τ_w for the receptor mediated uptake of ellipsoidal particles with aspect ratio Γ [adapted from Decuzzi and Ferrari, 2009].

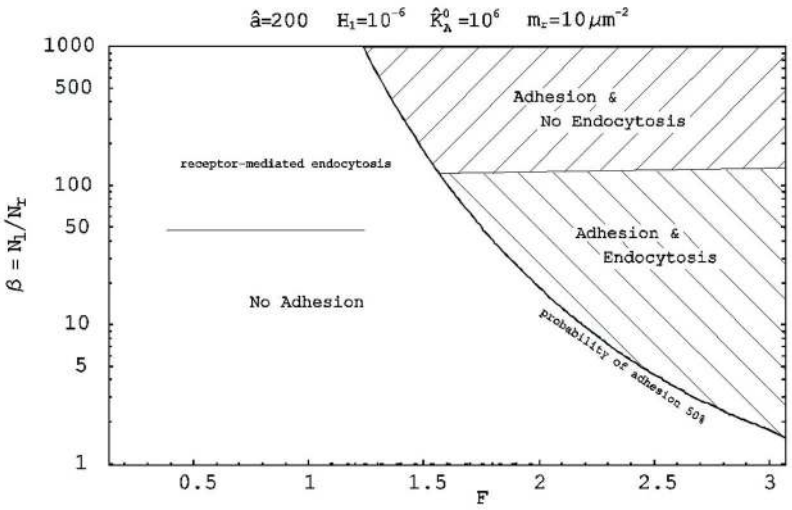

Fig. 7.
Design maps for spherical beads [adapted from Decuzzi and Ferrari, 2008]

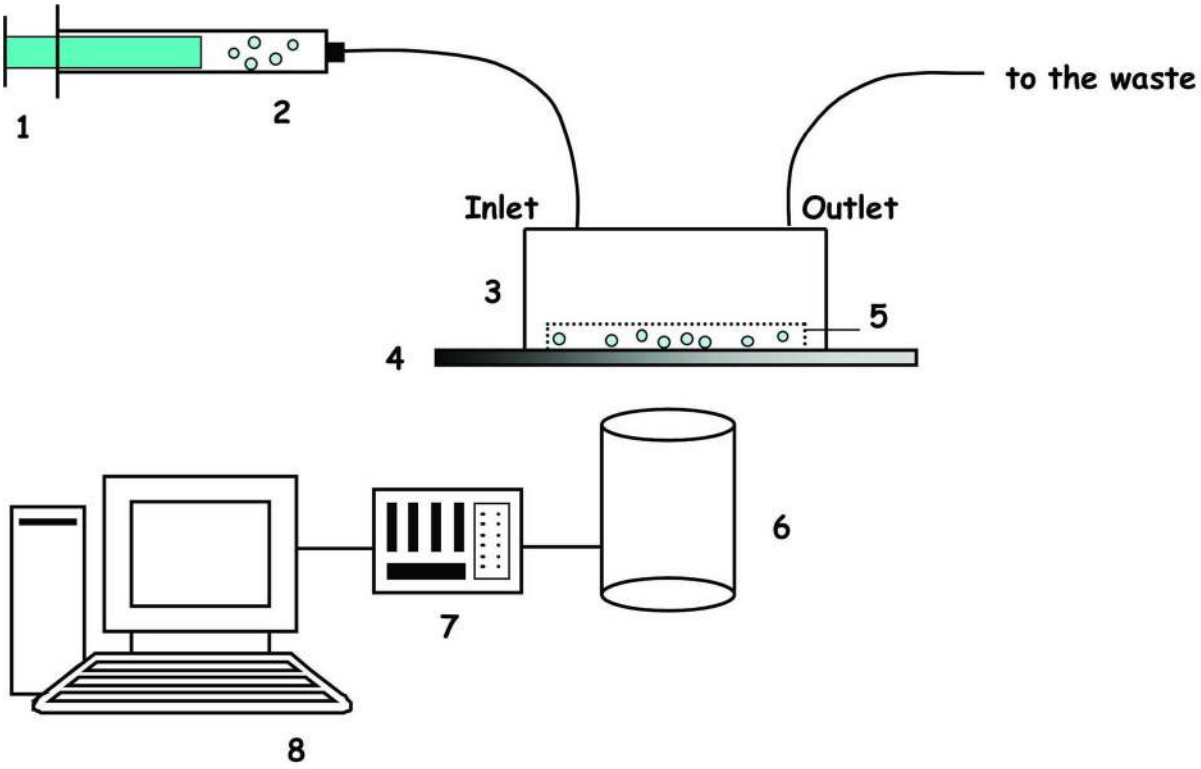

Fig. 8.

The experimental apparatus: 1. syringe (and pump); 2. nanovectors in solution, 3 flow chamber; 4. cell culture dish; 5. gasket; 6. microscope; 7. acquisition system; 8 PC

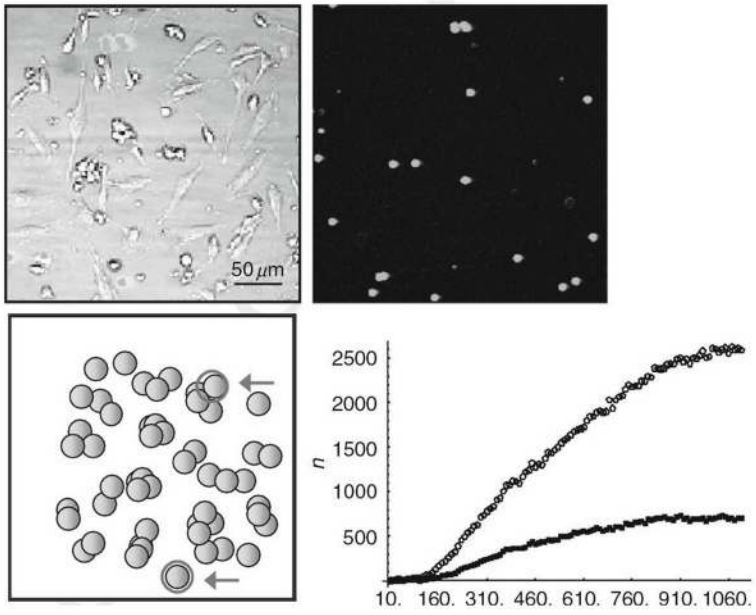

Fig. 9.

From left: Bright field and fluorescence images of 1 μm fluorescent particles adhering to a sub-confluent layer of Human Umbilical Vein endothelial Cells (HUVECs); fluorescent image; schematic for image analysis; number of adhering particles over time (Decuzzi et al., 2007).

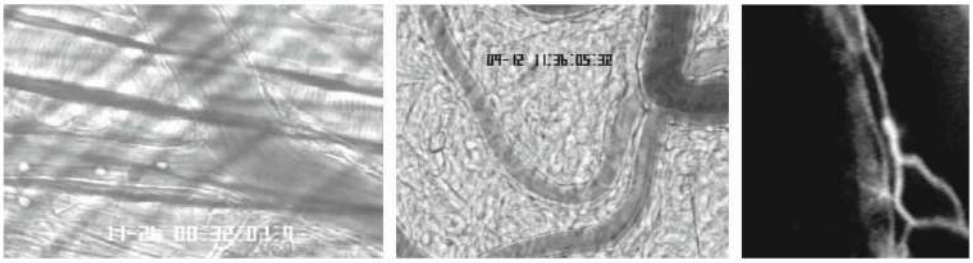

Fig. 10.

Intravital microscopy examples. A) Brightfiled imaging of mouse cremaster showing three rolling leukocytes (arrows) in a convergent venule. B) Brightfield imaging of rat mesentery with a convergent venule (ven.) and arteriole (art.). C) Epifluorescence image of limbal microvessels of the mouse cornea, following intravascular injection of a fluorescently-labeled macromolecule. Bar = 50 μm.

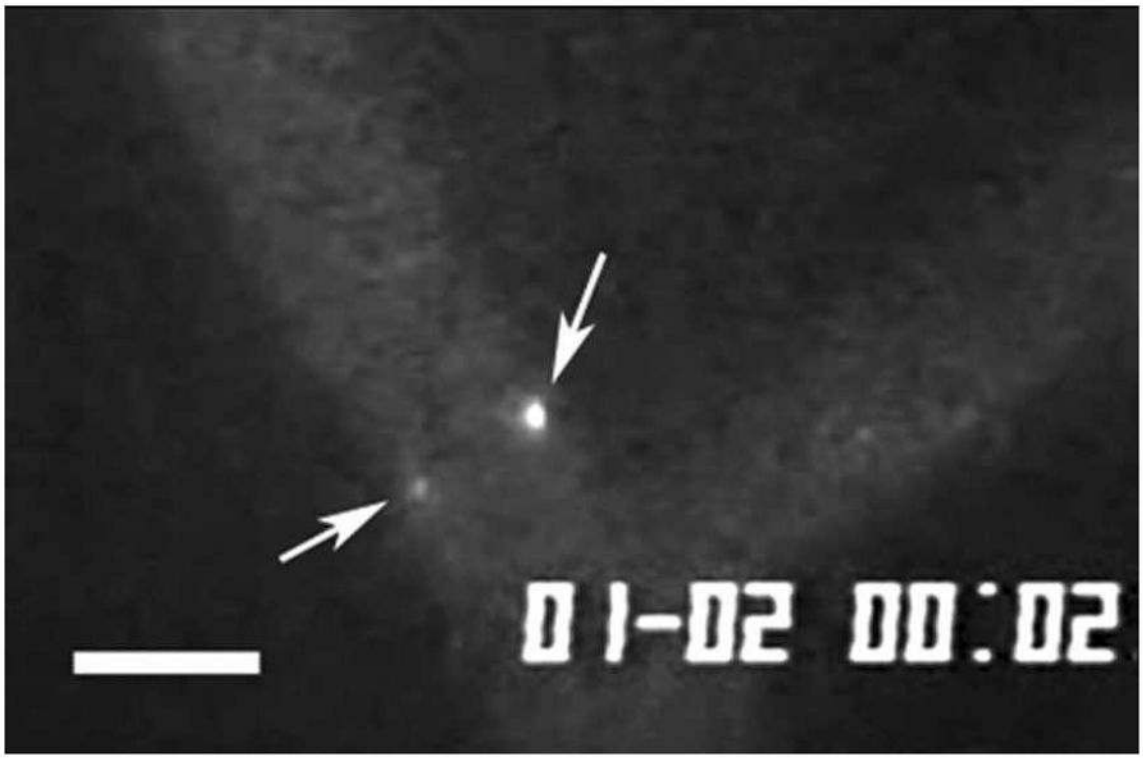

Fig. 11.

Two fluorescently-labeled microparticles (1 μm diameter, arrows) in a mouse cremaster arteriole. Bar = 20 μm

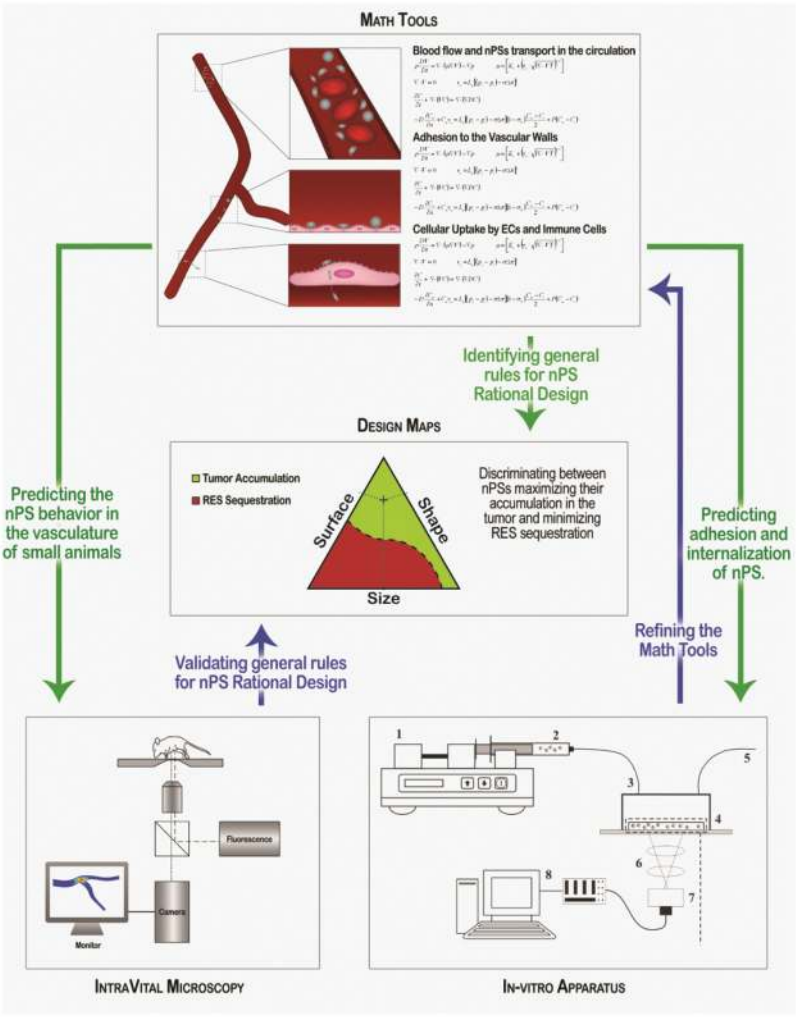

Fig. 12.

The integrated approach and the interaction among the three fundamental components.

Tab. 1

Hydraulic permeability of capillaries in various organs.

Organ	$L_p \times 10^{-3}$ (μm/Pa s)	Type of endothelium
Brain	3	Continuous
Skin	100	Continuous
Skeletal muscle	250	Continuous
Lung	340	Continuous
Heart	880	Continuous
Gastrointestinal tract	13,000	Fenestrated
Glomerulus in kidney	15,000	Fenestrated

Tab. 2

Physiologically relevant values for the parameters in Eq. (1) to (5)

	Symbol	Value
hydraulic conductivity	L_p^{normal}	3×10^{-12} *m*/(*Pa s*)
	L_p^{tumor}	3×10^{-11} *m*/(*Pa s*)
osmotic reflection coeff.	σ^{normal}	0.9
	σ^{tumor}	0
solute reflection coeff.	σ_F	0~0.9
diffusive permeability	P^{normal}	0
	P^{tumor}	10^{-12} ~ 10^{-18} *m/s*
oncotic pressure diff.	$\Delta\pi^{normal}$	2.5 *kPa*
	$\Delta\pi^{tumor}$	0
capillary pressure	p_c^{in}	4 *kPa*
	p_c^{out}	1 *kPa*
interstitial pressure	p_i^{normal}	−0.5 ~ 0.5 *kPa*
	p_i^{tumor}	0.5 ~ 1.0 *kPa*
particle radius	r	100 *nm*
fluid dynamic viscosity	μ	3.5×10^{-3} *Pa s*
fluid density	ρ	1.05×10^{3} *kg*/*m*^{3}
Boltzmann thermal energy	k_BT	4.142×10^{-21} *J*